

Correlated electrons systems on the Apollonian network

Andre M. C. Souza^{1,2} and Hans Herrmann^{3,4}

¹*Institut für Computerphysik, Universität Stuttgart, Pfaffenwaldring 27, 70569 Stuttgart, Germany*

²*Departamento de Física, Universidade Federal de Sergipe, 49100-000 Sao Cristovao-SE, Brazil*

³*Institut für Baustoffe, ETH Hönggerberg, HIF E 12, CH-8093 Zürich, Switzerland and*

⁴*Departamento de Física, Universidade Federal do Ceará, 60451-970 Fortaleza-CE, Brazil*

(Dated: March 23, 2022)

Strongly correlated electrons on an Apollonian network are studied using the Hubbard model. Ground-state and thermodynamic properties, including specific heat, magnetic susceptibility, spin-spin correlation function, double occupancy and one-electron transfer, are evaluated applying direct diagonalization and quantum Monte Carlo. The results support several types of magnetic behavior. In the strong-coupling limit, the quantum anisotropic spin $\frac{1}{2}$ Heisenberg model is used and the phase diagram is discussed using the renormalization group method. For ferromagnetic coupling, we always observe the existence of long-range order. For antiferromagnetic coupling, we find a paramagnetic phase for all finite temperatures.

PACS numbers: 71.27.+a, 71.10.Fd, 05.45.Df, 02.70.Ss

I. INTRODUCTION

Scale-invariant networks have been subject of intensive study in view of possible insights into inhomogeneous problems such as random magnets, surfaces, porous rocks, aerogels, sponges, etc. They are relevant to many different real complex situations like biological, social and technological systems [1, 2], where the structures can embody a particular graph, e.g., a scale free network. In this case, the fraction of sites with k connections follows a power law [3]. This topology has been found, in particular, on World Wide Web and Internet networks [4].

More recently, the area of scale-invariant networks has been highly motivated by the creation of a synthetic nanometer-scale Sierpinski hexagonal gasket, a self-similar fractal macromolecule [5]. New types of photoelectric cells, molecular batteries and energy storage may be possible. This perspective is relevant in view of the renewed interest in correlated electron systems on these networks, like studies of quantum magnetism, superconductivity, metal-insulator transition, etc. An important aspect that can be analyzed is the influence of the topology and the appearance of magnetic order.

In this paper, we investigate one family of free scale-invariant graphs, the Apollonian network [6, 7, 8]. The purpose is to examine correlated electrons on Apollonian networks. We explore the connection between the scale-invariant network topology and the magnetic properties of quantum magnetism models, namely, Hubbard and anisotropic spin $\frac{1}{2}$ Heisenberg models. We have examined the Hubbard model using the small cluster diagonalization [9, 10] and quantum Monte Carlo [11, 12]. The Heisenberg model is studied within a real-space renormalization group framework [13, 14, 15].

The construction of the Apollonian network has the topology of the contacts of an Apollonian packing of two-dimensional disks. As initial configuration we use, for an Apollonian packing, three mutually touching circles in-

scribed inside a circular space. The interstices of the initial disks define a curvilinear triangle to be filled. In the next iteration, four disks are inscribed, each touching all the sides of the corresponding curvilinear triangle. This process is repeated indefinitely by setting disks in the newly generated curvilinear triangles. The Apollonian packing is a fractal whose dimension has been estimated as 1.3057 [8].

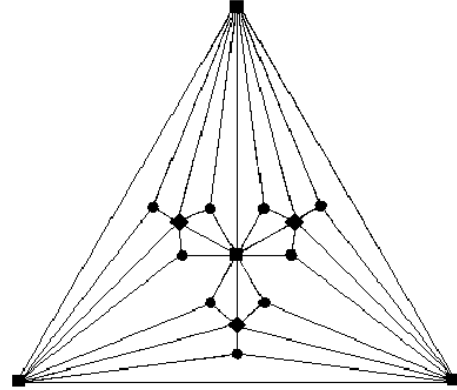


FIG. 1: First three generations of the Apollonian network. Sites represented by squares, diamonds and circles are introduced in the first, second and third generation.

The Apollonian network (AN) is derived from the two-dimensional Apollonian packing associating vertices with the circles and connecting two vertices if the corresponding circles touch. Fig 1 shows the first three generations of the AN. With this construction procedure one obtains a deterministic scale free network where the number of sites at iteration n is $(3^{n-1} + 5)/2$. Besides being a scale-free network, the AN has interesting properties like being Euclidean, matching and space-filling [6].

The organization of this paper is as follows. The models are briefly introduced in section II. The results

for ground-state and thermodynamic properties of the Hubbard model on AN are presented in section III and IV, respectively. The phase diagram of the quantum anisotropic Heisenberg model is discussed in section V and conclusions are presented in section VI.

II. MODELS

Our study of the magnetic properties on AN are based on the Hubbard model. The Hamiltonian of the Hubbard model is defined by

$$\mathcal{H}_u = -t \sum_{\langle ij \rangle \alpha} c_{i\alpha}^\dagger c_{j\alpha} + U \sum_i n_{i\uparrow} n_{i\downarrow}, \quad (1)$$

where $c_{i\alpha}^\dagger$, $c_{i\alpha}$ and $n_{i\alpha} \equiv c_{i\alpha}^\dagger c_{i\alpha}$ are respectively the creation, annihilation and number operators for an electron with spin α in an orbital localized at site i ; the $\langle ij \rangle$ sum runs over nearest-neighbor sites on AN [16].

The question of magnetic order in the one-band Hubbard model has been investigated by several authors and much controversy has arisen. In the strong-coupling limit a major part of the ferromagnetic phase is predicted. In this case, at half filling band, U is much larger than t , and the Hubbard model, using a suitable expansion in perturbation theory, is formally equivalent to the antiferromagnetic Heisenberg model. The Heisenberg exchange parameter J is written in terms of the Hubbard model parameters as $J = -4t^2/U$, where the Hamiltonian of the Heisenberg model is defined by

$$\mathcal{H}_e = -J \sum_{\langle ij \rangle} \vec{S}_i \cdot \vec{S}_j, \quad (2)$$

where \vec{S}_i is the total spin $\frac{1}{2}$ operator for the i th site. Here we study the anisotropic Heisenberg model to compare the behavior for different values of the anisotropy parameter [15].

III. GROUND-STATE PROPERTIES

We have obtained exact numerical results of the Hubbard model defined on second generation of the AN, corresponding to seven sites. We computed all the eigenvalues and eigenvectors of the Hamiltonian of Eq. 1 on a basis of states for which the occupation number is diagonal. We consider subspaces of fixed total azimuthal spin operator S_Z . Thus, the maximum possible dimension of the matrix to diagonalize is 1225.

Table I shows the results for the spin of the ground state. Until the half-filled band, the occurrence of a ferromagnetic state, where the total spin S is not minimum, can be found only for four electrons. In this case the ground state is threefold-degenerate corresponding to a triplet state of $S = 1$. This behavior can be explained considering the spectrum of the free electron system. Table II lists the single electron energies and degeneracies.

$n = 2$	$S = 0$, all U/t
$n = 3$	$S = 1/2$, all U/t
$n = 4$	$S = 1$, all U/t
$n = 5$	$S = 1/2$, all U/t
$n = 6$	$S = 0$, all U/t
$n = 7$	$S = 1/2$, all U/t
$n = 8$	$S = 0$, $U/t < 12.5$
	$S = 1$, $12.5 < U/t < 15.4$
	$S = 2$, $15.4 < U/t < 20.1$
	$S = 3$, $U/t > 20.1$
$n = 9$	$S = 1/2$, all U/t
$n = 10$	$S = 1$, $U/t < 8.44$
	$S = 2$, $U/t > 8.44$
$n = 11$	$S = 1/2$, $U/t < 0.44$
	$S = 3/2$, $U/t > 0.44$
$n = 12$	$S = 0$, $U/t < 0.57$
	$S = 1$, $U/t > 0.57$

TABLE I: Spin of the ground state as function of occupation number and U/t on the AN of 7 sites.

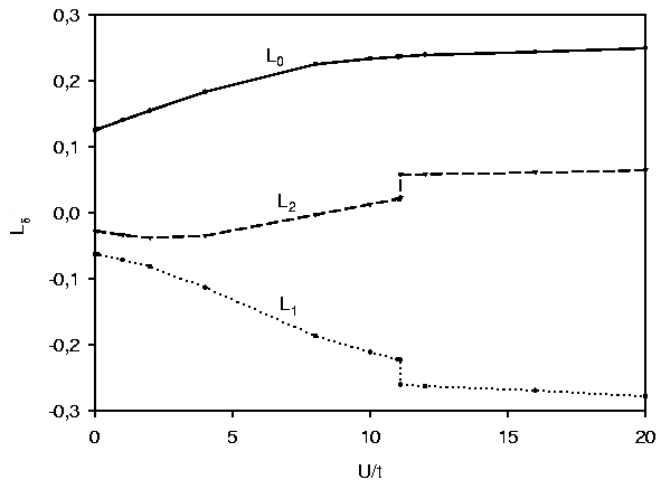


FIG. 2: Ground state spin-spin correlation function versus U/t for the half-filled band on the AN of 7 sites.

The double degeneracy in second level forms a triplet in lowest energy for the four electrons case. For two, three, five, six and seven electrons the ground state always has minimum spin. We observe that the Coulombian interaction does not favour the occurrence of a high spin ground state. If U/t is strong, the jumps of electrons decrease and a frustrated ordered antiferromagnet is favored. We easily see that the network is not bipartite, so its structure is antiferromagnetically frustrated. We find a similar competition, between interaction and frustration, in the low-temperature antiferromagnetic state on a triangular lattice [17].

Above the half-filled band we obtain a ferromagnetic ground-state. Nagaoka demonstrated that the ferromagnetism is expected for the antiferromagnetically frustrated structures in the half-filled band case with one excess electron and $U \rightarrow \infty$ [18]. Here, this limit repre-

E_1	$E_2 = E_3$	E_4	$E_5 = E_6$	E_7
-4.5114	-0.6180	0.7589	1.6180	1.7525

TABLE II: Energy levels E_i ($i=1, 2, \dots, 7$) of free electron system ($U/t = 0$) on the AN of 7 sites.

sents the eight electrons case for $U/t \gg 1$. We can see that if U/t increases the alignment of spins also increases, in such a manner that, for $U/t > 20.1$, the ferromagnetic state with the maximum total spin is the ground state. For more than eight electrons ferrimagnetism is possible, but not stronger than in the case of completely saturated ferromagnetism.

In general, the behavior of short(or long)-range ordering can be better observed studying the spin-spin correlation function. Considering the azimuthal spin operator on site i as $S_i^z = n_{i\uparrow} - n_{i\downarrow}$, the spin-spin correlation function is defined, for N sites, as

$$L_\delta = \frac{1}{4N} \sum_i S_i^z S_{i+\delta}^z. \quad (3)$$

The quantity L_0 , called local moment, depends on the magnitude of the difference between up and down electron spin at each site. It shows the degree of localization of electrons. For a completely localized system in which each site is occupied by a single electron (up or down), $L_0 = 1/4$, while for a non-interacting system $L_0 = 1/8$. L_δ ($\delta \neq 0$) is the correlation between the electron spins at different sites. They are related to the magnetic ordering. The results for the ground state spin-spin correlation function versus U/t in the half-filled band case are presented in Fig. 2. L_0 gradually increases if $U/t > 0$ increases, i.e., electrons gradually localize. L_1 has negative sign and increases if $U/t > 0$ increases and L_2 has a critical value for $U/t = 8$ where the behavior changes from negative to a positive sign. For $U/t > 8$, L_2 is positive, L_1 is negative, and an antiferromagnetic order appear. For $U/t = 11.1$ there is a change in the spatial symmetry of the ground state. It is important to observe the discontinuous change of L_1 and L_2 . This quantum transition point at $U/t = 11.1$ must not be a Mott metal-insulator transition because L_0 is continuous [9]. For $U/t \gg 1$, L_0 is approximately equal to $1/4$ and we can conclude that each site is occupied by just one electron. Our results indicate that the system can present a ferrimagnetic order, however, because the size of the network considered, the ferrimagnetic state has minimum spin $S = 1/2$, and we cannot have high spin ground state. For $U/t < 8$, L_2 is negative and the magnetic behavior of the ground state is more complex.

We analyse the wave function of the ground state, defining $P_k = |\Psi_{k0}|^2$, where $|\Psi_{k0}|$ is the n th component of the ground eigenstate. We define the total antiferromagnetic configuration ($k = AF$) such that sites introduced in the first generation on AN (represented by squares in Fig. 1) are occupied by electrons of a type of spin and sites introduced in second generation (represented by diamonds in Fig. 1) are occupied by elec-

trons of opposite spin. We observe that $P_{AF}/P_k > 2$ for $U/t = 0$ and increases to $P_{AF}/P_k > 15$ if $U/t = 8$, for all $k \neq AF$, i.e., the total antiferromagnetic configuration P_{AF} is approximately 2 times for $U/t = 0$ and 15 times for $U/t = 8$, more probable than any another configuration. Thus, we can construct a physical picture where the ground state has an antiferromagnetic order (frustrated) at any U/t .

IV. THERMODYNAMIC PROPERTIES

On one hand, we study the thermodynamic properties of the half-filled band Hubbard model using the method of small-cluster exact-diagonalization calculations in the grand canonical ensemble [10]. We have calculated all eigenvalues and eigenfunctions for AN of 7 sites. On the other hand, we study lattices of 63 and 124 sites using the grand canonical quantum Monte Carlo method [11, 12]. We used a discrete Hubbard-Stratonovich transformation to convert the problem into one of free particles interacting with a time-dependent Ising field, together with an exact updating algorithm for the fermions Green's function to compute the relative weights of the Ising configurations.

We consider several values of U/t for all the studied thermodynamic properties. We determine with considerable accuracy the temperature dependence of the spin-spin correlation functions, spin susceptibility, specific heat, double occupancy and one electron transfer.

The temperature dependence of L_0 , L_1 and L_2 for some typical values of U/t is shown in Figs. 3a-3c. If U/t increases, L_0 gradually increases for $U/t > 0$, indicating that electrons are gradually localizing. At high temperature L_0 gradually decreases and electrons gradually delocalize. At very low temperatures, the temperature dependence with negative signs of L_1 induces an antiferromagnetic ordering. The inset in Fig. 3b shows Monte Carlo results for AN with 7, 43 and 124 sites and $U/t = 1$. Results for 43 and 124 sites do not reveal any new behavior, however, the antiferromagnetic ordering increases. We observe that the properties obtained for 7 sites must be qualitatively equivalent to those for larger AN. We observe a competition between interaction and frustration in the ordered antiferromagnetic state by the analysis of L_2 . For small or intermediary U/t , the negative sign of L_2 is a result of the frustrated structure of AN, disfavoring the antiferromagnetic order. For $U/t \gg 1$, L_2 has positive sign, showing that the strong electron interaction favors the antiferromagnetic order.

Fig. 4 shows the temperature dependence of the magnetic susceptibility, χ . The Curie-Weiss behavior, $\chi \propto 1/(T - \theta)$, is observed for high temperatures. For small and intermediary U/t the curves present a peak. The temperature associated with the peak of χ corresponds approximately to the rapid decay of L_1 and L_2 , and is a consequence of the collective excitations that lead to the destruction of the antiferromagnetic order [9].

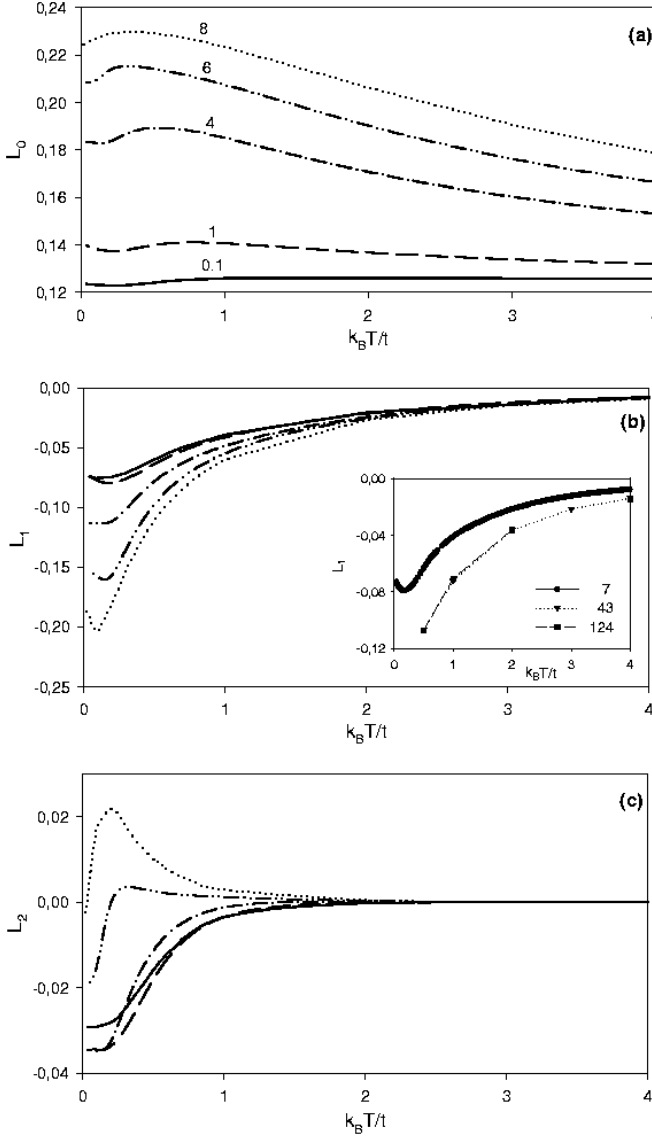


FIG. 3: Correlation functions L_δ vs. temperature with $U/t = 0.1, 1, 6$ and 8 for the AN of 7 sites. (a) L_0 ; (b) L_1 ; (c) L_2 . In the inset of (b), L_1 with $U/t = 1$ for 7, 43 and 124 sites on AN using Monte Carlo method.

Here the ground state has spin $S = 1/2$ and χ must go to infinity at temperature $T = 0$. The susceptibility χ with $U/t = 1$ for 7, 43 and 124 sites on AN using Monte Carlo method is shown in the inset of Fig. 4. In this case, we do not see any discrepancy between the results for different clusters.

The temperature dependence of the specific heat is shown in Fig. 5 for typical values of U/t . For small values of U/t there is a peak in the specific heat. Increasing U/t , the peak splits into two, which reflects a rearrangement of the fermionic structure in the system. The low-temperature peak arises due to low-lying collective excitations, while the high-temperature broad peak comes from single-particle excitations. This behavior is

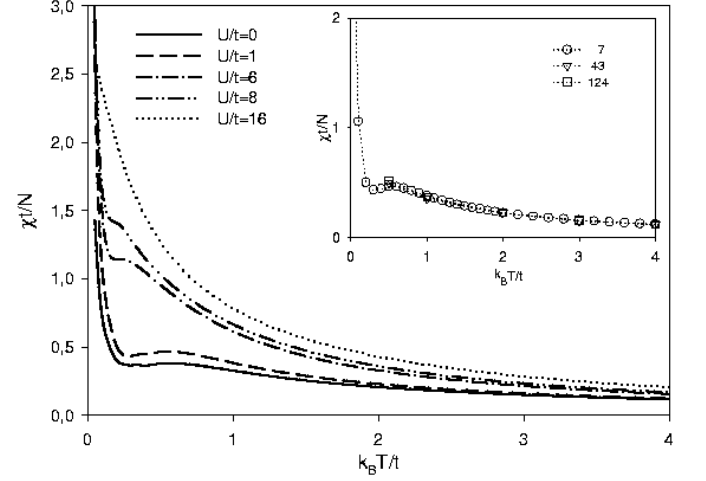


FIG. 4: Magnetic susceptibility as a function of temperature with $U/t = 0, 0.5, 4$, and 8 for the AN of 7 sites. Inset: Magnetic susceptibility with $U/t = 1$ for 7, 43 and 124 sites on AN using Monte Carlo method.

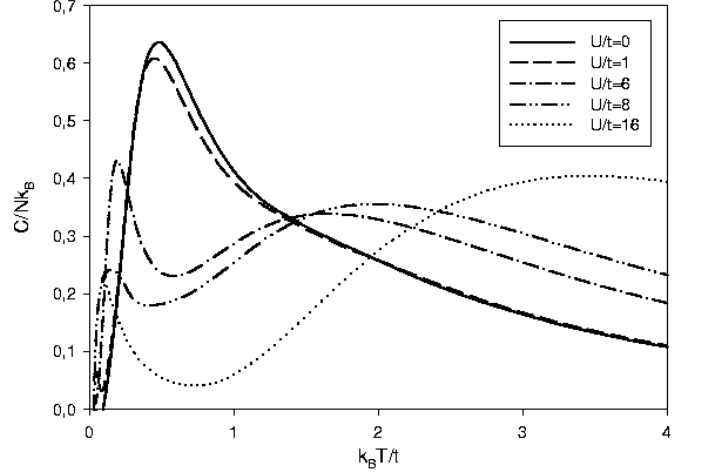


FIG. 5: Specific heat $C/(Nk_B)$ as a function of temperature with $U/t = 0, 0.5, 4$ and 8 for the AN of 7 sites.

quite general and has been noticed for different structures [9, 10].

Next, we study the thermal average of the double occupancy $d = \frac{1}{N} \sum_i n_{i\uparrow} n_{i\downarrow}$ and of the one-electron transfer defined by

$$j = \sum_{\langle ij \rangle \alpha} c_{i\alpha}^\dagger c_{j\alpha} = \frac{Ud - \mathcal{H}}{t}. \quad (4)$$

Fig. 6 shows the temperature dependence of j and d (inset) with $U/t = 0.1, 1$ and 4 for the AN with 124 sites. Clearly these functions are related to the local moment. It is easy to show that for the half-filled band $d = (1 - 4L_0)/2$. If U/t increases, the local moment increases (see Fig. 3a) and the double occupation and one-electron transfer decrease. In the strong coupling

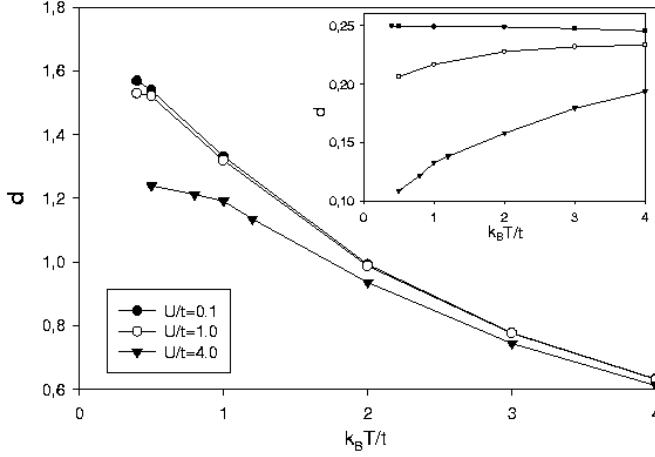


FIG. 6: One-electron transfer j as a function of temperature with $U/t = 0.1, 1$ and 4 for the AN of 124 sites. Inset: Double occupancy d as a function of temperature.

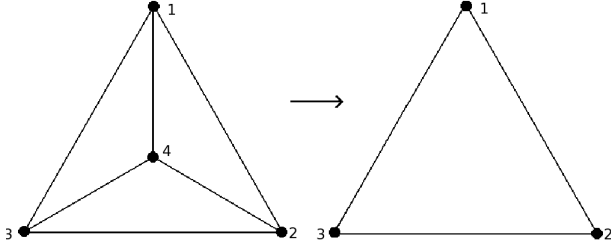


FIG. 7: Renormalization group transformation associated to the AN.

limit ($U/t \gg 1$) each site is occupied by just one electron and the electronic itinerancy vanishes. This region is characterized by localized magnetism and we can apply the Heisenberg model.

V. LOCALIZED MAGNETISM: RENORMALIZATION GROUP APPROACH

The fractal and self-similar nature of scale-invariant networks, generated through a recursive procedure, offer an appropriated way to get rigorous result at the phase transition. The difficulty with the spin-decimation process which leads to the renormalization-group equation as found on Bravais lattices due to parameter proliferation, disappears on scale-invariant networks [20, 21]. Due to the fact that fractal lattices are characterized by dilation invariance but do not have translational invariance, the study on these networks can with restriction be used to model Bravais lattices. Particularly self-similar networks can mimic Bravais lattices for some magnetic models, providing equal critical temperatures and exponents [21, 22].

The real-space renormalization group (RG) approach has been applied with success to the study of the

anisotropic spin $\frac{1}{2}$ Heisenberg model on self-dual hierarchical lattices [13, 14, 15]. Here, we apply this analysis on AN. It is defined by the cluster transformation process, preserving the Hamiltonian form, as illustrated in Fig. 7.

The dimensionless Hamiltonian is defined by

$$h = -\beta\mathcal{H} = \frac{4J}{k_B T} \sum_{\langle ij \rangle} [(1-\Delta)(S_i^x S_j^x + S_i^y S_j^y) + S_i^z S_j^z], \quad (5)$$

where $\beta \equiv 1/k_B T$, $\langle ij \rangle$ denotes first-neighboring lattice sites, Δ is the anisotropy parameter and the S_i^α ($\alpha = x, y, z$) is the α -spin $1/2$ operator on site i . The RG recurrence equation is obtained by imposing

$$\exp(h'_{123} + C) = \text{Tr}_{\text{site 4}} \exp(h_{1234}) \quad (6)$$

where h_{1234} and h'_{123} are, respectively, the Hamiltonian of the four-site cluster and of the renormalized three-site cluster, shown in Fig. 7. To make the RG equation possible, an additive constant C has been included. The RG Eq. 6 establishes the relation between the set of parameters (J, Δ) and the set of renormalized parameters (J', Δ') . The non-commutativity between the Hamiltonians associated with neighboring clusters is neglect, and therefore our results are approximations for all temperatures, only being asymptotically exact at high temperatures [14].

Defining $K \equiv J/k_B T$ and expanding $\exp(h'_{123})$ as

$$\exp(h'_{123} + C) = a' + 4b'(S_1^x S_2^x + S_1^y S_2^y + S_1^x S_3^x + S_1^y S_3^y + S_2^x S_3^x + S_2^y S_3^y) + 4c'(S_1^z S_2^z + S_1^z S_3^z + S_2^z S_3^z), \quad (7)$$

we obtain that

$$\begin{aligned} 4K' &= \ln\left(\frac{a' + 3c'}{a' - c' - 2b'}\right) + \frac{1}{3} \ln\left(\frac{c' - a' + 2b'}{c' - a' - 4b'}\right) \\ 6K' \Delta' &= \ln\left(\frac{c' - a' - 4b'}{c' - a' + 2b'}\right) \\ C &= -3K' + \ln(a' + 3c'). \end{aligned} \quad (8)$$

Analogously,

$$\begin{aligned} \exp(h_{1234}) &= a + 4 \sum_{(i < j)} [b(S_i^x S_j^x + S_i^y S_j^y) + c S_i^z S_j^z] \\ &\quad + 16 \sum_{(i < j) \neq (k < l)} [d(S_i^x S_j^x + S_i^y S_j^y) S_k^z S_l^z \\ &\quad + g(S_i^x S_j^x + S_i^y S_j^y)(S_k^x S_l^x + S_k^y S_l^y)] \\ &\quad + 16 f S_1^z S_2^z S_3^z S_4^z \end{aligned} \quad (9)$$

where a, b, c, d, g and f are functions of K and Δ . It is easy to see from Eq. 6 that $a' = 2a$, $b' = 2b$ and $c' = 2c$. The set of parameters (K', Δ') as functions of (K, Δ) can be determined by diagonalizing h_{123} and h_{1234} and using Eqs. 6-9. After some calculus we obtain the analytical RG equation as

$$\begin{aligned} a' &= \frac{1}{4} [e^{6K} + e^{6K\Delta} + 3e^{-2K\Delta} + \frac{e^{-2K}}{2} (3 + e^{8K\Delta} + 2e^{-4K\Delta})] \\ b' &= \frac{1}{4} [\frac{e^{6K\Delta} - e^{-2K\Delta}}{2} + \frac{e^{-2K}}{3} (e^{8K\Delta} - e^{-4K\Delta})] \\ c' &= \frac{1}{4} [e^{6K} - \frac{e^{-2K}}{6} (3 + e^{8K\Delta} + 2e^{-4K\Delta})] \end{aligned} \quad (10)$$

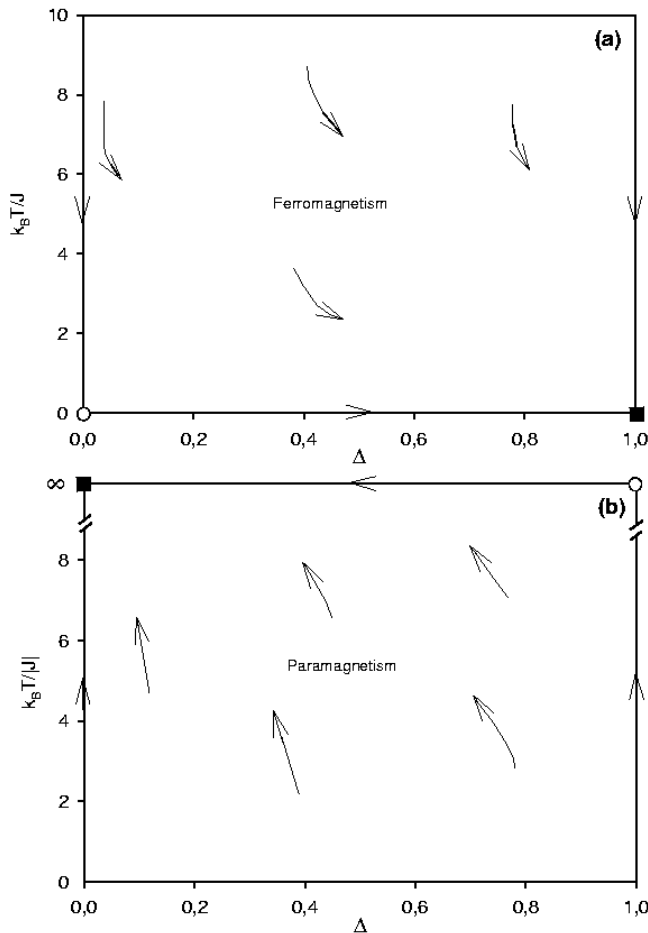


FIG. 8: Flow diagram for the Apollonian cell of Fig. 7. Open circles, and full squares respectively, denote, the semi-stable and fully stable fixed points. (a) ferromagnetic case ($J > 0$). (b) antiferromagnetic ($J < 0$) case.

where K', Δ' are functions of c', a', b' given by Eq. 8. We observe that the Ising and isotropic Heisenberg models are mapped into themselves. The RG recurrence is simplified as

$$k' = \frac{1}{4} \ln \left(\frac{1 + e^{6K}}{1 + e^{-2K}} \right) \quad (11)$$

and

$$k' = \frac{1}{6} \ln \left(\frac{3 + 5e^{8K}}{6 + 2e^{-4K}} \right) \quad (12)$$

corresponding to the Ising ($\Delta = 1$) and the isotropic Heisenberg ($\Delta = 0$) limits, respectively.

Fig. 8 shows the phase diagram in the $(k_B T/J, \Delta)$ space. In the ferromagnetic case ($k_B T/J > 0$), we always observe the existence of ferromagnetism (F) independent of Δ . This result has been found on AN for the Ising model using the transfer matrix method [7] and on other scale-free lattices [19]. Those results agree very well with ours. Here, we observe that the quantum fluctuations of the XY part of our Hamiltonian does not destroy this ordering generated by the topology of the AN. In the antiferromagnetic case ($k_B T/J < 0$), we verify the non-existence of the ordered phase for all Δ at finite T . Again, the results obtained are similar and consistent with the Ising limit [7].

VI. CONCLUSIONS

In conclusion, we have analyzed strongly correlated electron systems on AN. The ground state and thermodynamic properties of the Hubbard model have been studied using exact diagonalization calculations and quantum Monte Carlo. The dependence on the ratio U/t of the specific heat, the magnetic susceptibility, the spin-spin correlation function, the double occupancy and the one-electron transfer support several types of magnetic behavior. We have also studied the magnetic properties of the anisotropic spin $\frac{1}{2}$ Heisenberg model on the AN using the real-space RG approach. For ferromagnetic coupling, we always observe the existence of ferromagnetism independent on temperature and anisotropy parameter Δ . As opposed to other structures [14, 15], the topology of the AN favors the ferromagnetic order and the quantum fluctuations do not destroy this ordering. For antiferromagnetic coupling, we find a paramagnetic phase for all Δ at finite T . A similar result has been found on AN for the Ising model using the transfer matrix method [7].

Acknowledgments

Authors thank P. G. Lind and E. Parteli for their generous help. This work was supported by CNPq (Brazil), DAAD (Germany) and the Max Planck prize.

- [1] R. Albert and A. L. Barabási, *Rev. Mod. Phys.* **74**, 47 (2002).
- [2] S. N. Dorogovtsev and J. F. F. Mendes, *Evolution of Network From Biological Nets to the Internet and WWW* (Oxford University Press, Oxford, 2003); S. N. Dorogovtsev and J. F. F. Mendes, *Adv. Phys.* **51**, 1079 (2002).
- [3] A. L. Barabási and R. Albert, *Science* **286**, 509 (1999).

- [4] M. Faloutsos, P. Faloutsos, and C. Faloutsos, *Comput. Commun. Rev.* **29**, 251 (1999).
- [5] G. R. Newkome, P. Wang, C. N. Moorefield, T. J. Cho, P. Mohapatra, S. Li, S. H. Hwang, O. Lukyanova, L. Echegoyen, J. A. Palagallo, V. Iancu, S. W. Hla, *Science* (2006).
- [6] J. S. Andrade Jr., H. J. Herrmann, R. F. S. Andrade,

- and L. R. da Silva, Phys. Rev. Lett. **94**, 018702 (2005).
- [7] R. F. S. Andrade and H. J. Herrmann, Phys. Rev. E **71**, 056131 (2005).
 - [8] J. P. K. Doye and C. P. Massen, Phys. Rev. E **71**, 016128 (2005).
 - [9] J. Callaway, D. P. Chen, and R. Tang, Phys. Rev. B **35**, 3705 (1987); J. Callaway, D. P. Chen, and Y. Zhang, Phys. Rev. B **36**, 2084 (1987).
 - [10] C. A. Macedo and A. M. C. Souza, Phys. Rev. B **65**, 153109 (2002).
 - [11] J. E. Hirsch, Phys. Rev. B **31**, 4403 (1985).
 - [12] C. A. Macedo and A. M. C. Souza, Physica B **354**, 290 (2004); A. M. C. Souza and C. A. Macedo, J. Magn. Mater. **226**, 2026 (2001).
 - [13] A. O. Caride, C. Tsallis, and S. I. Zanette, Phys. Rev. Lett. **51**, 145 (1983).
 - [14] A. M. Mariz, C. Tsallis, and A. O. Caride, J. Phys. C **18**, 4189 (1985).
 - [15] A. M. C. Souza, Phys. Rev. B **48**, 3744 (1993).
 - [16] R. F. S. Andrade and J. G. V. Miranda, Physica A **356**, 1 (2005).
 - [17] A. Singh, Phys. Rev. B **71**, 214406 (2005).
 - [18] Y. Nagaoka, Phys. Rev. **147**, 392 (1966).
 - [19] A. Aleksiejuka, J. A. Holyst, and D. Stauffer, Physica A **310**, 260 (2002).
 - [20] Z. R. Yang, Phys. Rev. B **38**, 728 (1988).
 - [21] M. Kaufman and R. B. Griffiths, Phys. Rev. B **24**, 496 (1981).
 - [22] A. M. C. Souza and C. Tsallis, Phys. Rev. B **47**, 11940 (1993).